**Research Article**

Shulei Li*, Fu Deng*, Lidan Zhou, Zhenxu Lin, Mingcheng Panmai, Shimei Liu, Yuheng Mao, Jinshan Luo, Jin Xiang, Jun Dai, Yunbao Zheng and Sheng Lan*

# Revealing defect-bound excitons in $WS_2$ monolayer at room temperature by exploiting the transverse electric polarized wave supported by a $Si_3N_4$/Ag heterostructure

https://doi.org/10.1515/nanoph-2023-0560
Received September 1, 2023; accepted November 13, 2023; published online November 22, 2023

**Abstract:** Two-dimensional (2D) transition metal dichalcogenide (TMDC) monolayers are promising materials for light-emitting devices due to their excellent electric and optical properties. However, defects are inevitably introduced in the fabrication of TMDC monolayers, significantly influencing their emission properties. Although photoluminescence (PL) is considered as an effective tool for investigating the defects in TMDC monolayers. However, the PL from the defect-bound excitons is revealed only at low temperatures. Here, we show that the PL from the defect-bound excitons in a $WS_2$ monolayer can be effectively revealed at room temperature by exploiting the transverse electric polarized wave supported by a $Si_3N_4$/Ag heterostructure. It is revealed that the defect-bound excitons in all possible positions of the $WS_2$ monolayer can be effectively excited by the TE wave with significantly enhanced in-plane electric field localized on the surface of the $Si_3N_4$ layer. In addition, the emission from defect-bound excitons can propagate to the collection point with small attenuation. More importantly, the exciton dynamics in the $WS_2$ monolayer can be modified by the $Si_3N_4$/Ag heterostructure, allowing the simultaneous excitation of neutral excitons, charge excitons (trions), and defect-bound excitons in the $WS_2$ monolayer attached on the $Si_3N_4$/Ag heterostructure. We inspect the PL spectra obtained at different positions and find that the relative intensity of defect-bound excitons depends on the collection position. We also examine the dependences of the PL intensity and bandwidth on the excitation power for the three types of excitons. It is found that they exhibit different behaviors from those observed in the optical measurements by using the traditional excitation method. Our findings suggest a new way for exciting and studying the dynamics of multi-excitons at room temperature and indicate the potential applications of the TE wave in probing the defects in TMDC monolayers.

**Keywords:** monolayer transition-metal dichalcogenides; dielectric-metal heterostructure; transverse-electric-polarized wave; defect-bound exciton; photoluminescence patterns

***Corresponding authors: Shulei Li**, School of Optoelectronic Engineering, Guangdong Polytechnic Normal University, Guangzhou 510665, China, E-mail:shuleili@gpnu.edu.cn. https://orcid.org/0000-0001-9346-3773; **Fu Deng**, Department of Physics, Hong Kong University of Science and Technology, Kowloon, Hong Kong, China, E-mail: fu_deng@foxmail.com; and **Sheng Lan**, Guangdong Provincial Key Laboratory of Nanophotonic Functional Materials and Devices, School of Information and Optoelectronic Science and Engineering, South China Normal University, Guangzhou 510006, China, E-mail: slan@scnu.edu.cn

**Lidan Zhou**, State Key Laboratory of Optoelectronic Materials and Technologies and School of Electronics and Information Technology, Sun Yat-Sen University, Guangzhou 51006, China

**Zhenxu Lin**, **Mingcheng Panmai**, **Shimei Liu**, **Yuheng Mao and Jinshan Luo**, Guangdong Provincial Key Laboratory of Nanophotonic Functional Materials and Devices, School of Information and Optoelectronic Science and Engineering, South China Normal University, Guangzhou 510006, China. https://orcid.org/0000-0001-5704-095X (S. Liu)

**Jin Xiang**, Key Laboratory of Optoelectronic Technology and Systems (Chongqing University), Ministry of Education, School of Optoelectronic Engineering, Chongqing University, Chongqing 400044, China

**Jun Dai and Yunbao Zheng**, School of Optoelectronic Engineering, Guangdong Polytechnic Normal University, Guangzhou 510665, China

## 1 Introduction

Monolayer transition-metal dichalcogenides (TMDCs) have gained enormous research interest because of their unique electronic and optical properties, such as strong nonlinear effect [1–4], complex excitons response and valley selective

properties [5–9]. These properties make them important in light–matter interaction and optoelectronic applications [10–19]. Nowadays, monolayer TMDCs with large sizes can be obtained by using the chemical vapor deposition (CVD) method. As a result, hybrid structures composed of metasurfaces and monolayer TMDCs, in which light–matter interaction is greatly enhanced for various applications [20, 21], can be readily fabricated. However, previous studies indicate the existence of various intrinsic/extrinsic defects in monolayer TMDCs grown by the CVD method, such as vacancies, substitutional impurities, grain boundaries, and adatoms [22, 23], based on optically and chemically modulated methods [6, 7, 9, 20, 24, 25] and solution-based liquid-phase exfoliation. These defects exhibit a significant impact on the optical and optoelectronic properties of monolayer TMDCs [23, 26]. While defects are not always detrimental, it is known that point defects in a semiconductor can act as efficient traps to capture free carriers and localize excitons, strongly influencing the transport and optical properties of the host material [27–30]. In particular, such traps become more efficient in low-dimensional materials [26]. Since design and engineering of defects provide a new route for realizing functional properties of monolayer TMDCs, it has become a research hotspot in recent years.

Many gas molecules and chemical substances can effectively functionalize the surface of a two-dimensional material by adjusting defect-induced doping or repairing lattice structure, leading to enhanced luminescence and photoresponse [7, 22, 31–34]. Ion irradiation and plasma treatment are confirmed to be effective methods for creating atomic defects in two-dimensional materials, such as graphene [35], $WS_2$ [36], $MoS_2$ [37], $WSe_2$ [38, 39], $ReS_2$ [40], etc. For instance, site-controlled single-photon emitters in monolayer $WSe_2$ with high yield was successfully demonstrated [38]. With the rapid progress in the integration of monolayer TMDCs in practical devices, it is highly desirable to understand the physical properties of the defects in monolayer TMDCs and optical characterization appears to be an effective tool to achieve this goal.

Currently, the main techniques used to characterize the defects in monolayer TMDCs include electron beam imaging (e.g., scanning electron microscopy or SEM and transmission electron microscopy or TEM) and fluorescence spectroscopy [22]. Although electron beam imaging provides images at the nanoscale, the introduction of defects is generally inevitable [41]. Therefore, fluorescence characterization, with advantages of high sensitivity, nondestructiveness, and real-time capability, has been widely used [9, 31]. In the photoluminescence (PL) of monolayer TMDCs measured at low temperatures, a new peak was revealed at the long-wavelength side of the neutral excitons. It was attributed to the emission from excitons bound to defects. Unfortunately, the emission from such defect-bound excitons disappears in the PL spectra of monolayer TMDCs at room temperature, making it difficult to study their physical properties.

Physically, the disappearance of the emission from defect-bound excitons is caused by the activation of trapped excitons at room temperature. In order to reveal the emission from defect-bound excitons at room temperature, one needs to enhance the radiative recombination rate of defect-bound excitons, which can be realized by the so-called Purcell effect [42, 43]. In practice, metasurfaces with large field enhancements have been employed to enhance the PL from excitons [17, 44, 45]. However, the fabrication of metasurfaces is complicated and the integration of metasurfaces with monolayer TMDCs is difficult. In comparison, planar waveguide structures without any complex patterning process can also provide electric field enhancement used to modify the exciton dynamics in monolayer TMDCs. On the other hand, the emission from defect-bound excitons can be enhanced by exciting a monolayer TMDC with a large size attached on a planar waveguide structure. Since the self-absorption effect is much weaker for defect-bound excitons as compared with neutral excitions, the emission from defect-bound excitons can propagate a longer distance [46]. As result, the emission from defect-bound excitons is enhanced at the collection point because of its nonlocal feature. In a previous study, we showed that a dielectric-metal heterostructure composed of a $Si_3N_4$ layer and a thin Ag film can support transverse electric (TE) polarized waves localized on the surface of the $Si_3N_4$ layer. Owing to the enhancement in the in-plane electric field, strong coupling between the TE wave and the two excitons in a $WS_2$ monolayer attached on the $Si_3N_4$/Ag heterostructure was successfully demonstrated [47, 48]. Therefore, it is interesting to investigate the exciton dynamics in monolayer TMDCs excited by the TE wave supported by a dielectric-metal heterostructure.

In this work, we convert the excitation laser light into the TE wave propagating on a $Si_3N_4$/Ag heterostructure and excite a $WS_2$ monolayer attached on the heterostructure. In this way, we reveal simultaneously the emissions from neutral excitons ($X_A$), charge excitons (trions) ($X_T$), and defect-bound excitons ($X_D$) in the PL spectrum of the $WS_2$ monolayer at room temperature. We examine the dependences of the emission intensities from the three excitons on the excitation position and excitation intensity. Our

findings suggest a new way to excite the defect-bound excitons in $WS_2$ monolayer and investigate multi-exciton physics at room temperature.

## 2 Results and discussion

Monolayer $WS_2$ exhibits a strong exciton resonance in the visible light spectrum. Thus, a laser beam with in-plane polarization will greatly boost the interaction with a $WS_2$ monolayer, leading to enhanced PL intensity. In Figure 1a, we show schematically the interaction of a TE wave generated on the surface of a $Si_3N_4$/Ag heterostructure with a $WS_2$ monolayer attached on the heterostructure. The heterostructure is composed of a 50-nm-thick Ag film deposited on a $SiO_2$ substrate followed by a 100-nm-thick $Si_3N_4$ layer. Physically, the TE waves supported by the $Si_3N_4$/Ag heterostructure belong to substrate-modulated waveguide modes, similar to those described in previous studies [47, 48]. In this case, the whole $WS_2$ monolayer can be excited by the TE wave localized on the surface of the $Si_3N_4$ layer [48] (see Figure S1 in the Supporting Information). It implies the generation of defect-bound excitons in all possible locations. In addition, the exciton dynamics in the $WS_2$ monolayer will be modified by the $Si_3N_4$/Ag heterostructure. Finally, the emissions from defect-bound excitons at different locations

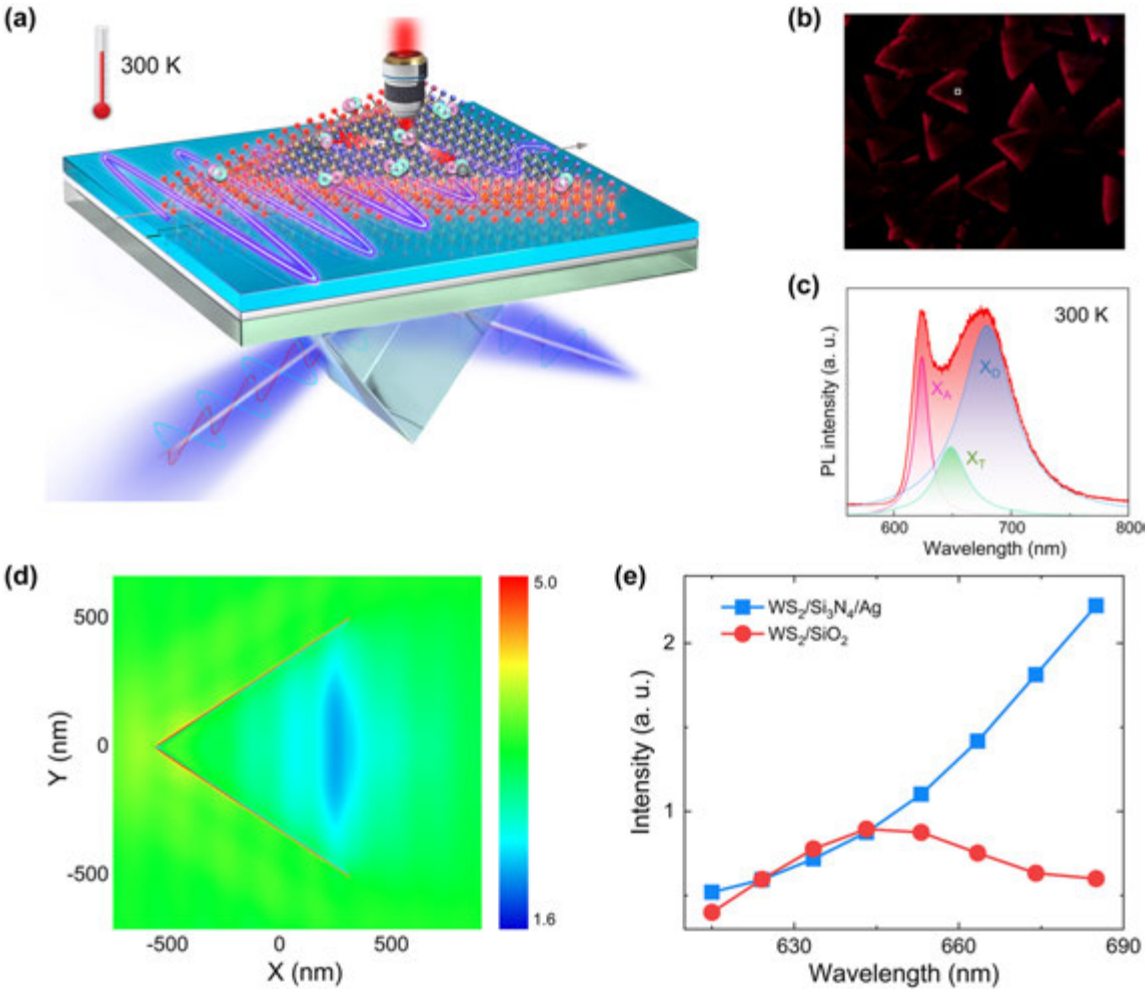


**Figure 1:** PL spectra of monolayer $WS_2$ from TE wave excitation. (a) Schematic showing the excitation of a $WS_2$ monolayer placed on a $Si_3N_4$/Ag heterostructure by coupling the laser light as a TE wave propagating on the heterostructure. The emissions from defect-bound excitons at different locations can be collected by an objective due to the existence of the waveguide structure. (b) Optical image of triangular $WS_2$ monolayers placed on $Si_3N_4$/Ag heterostructure and excited by 405-nm laser light propagating as a TE wave. (c) Typical PL spectrum of a $WS_2$ monolayers placed on the $Si_3N_4$/Ag heterostructure. Also shown are the fitting of the PL spectrum by Lorentz lineshapes. (d) In-plane electric field distribution ($E_{xy}$) calculated for a $WS_2$ monolayer placed on the $Si_3N_4$/Ag heterostructure. (e) Dependence of the radiation intensity on the wavelength calculated for a $WS_2$ monolayer placed on the $Si_3N_4$/Ag heterostructure and a $SiO_2$ substrate.

can propagate to the collecting point with small attenuation, leading to an enhanced intensity in the PL spectrum (see Figure S2 in the Supporting Information). In Figure 1b, we show the optical images of triangular $WS_2$ monolayers recorded by using a charge coupled device (CCD). In this case, $WS_2$ monolayers are excited by 405-nm laser light coupled into the $Si_3N_4$/Ag heterostructure as a TE wave at an incident angle of $\theta = 80°$ (see Figure 1a). It is noticed that each $WS_2$ monolayer emits red PL with enhanced intensity at left-side edges. In Figure 1c, we present a typical PL spectrum collected from a point on a $WS_2$ monolayer by using an objective and analyzed by using a spectrometer at room temperature (see Figure 1a). It can be fitted by three Lorentz lineshapes, which corresponds to the emissions from neural excitons, charge excitons and defect-bound excitons respectively. The PL peak at ∼680 nm is attributed to the emission from defect-bound excitons. This assignment is confirmed by the experiment described in the following. Comparing with the conventional point excitation which exhibits only the emission from neutral excitons, the excitation of $WS_2$ monolayer by using TE wave reported in this work provides a simple and effective way for revealing defect-bound excitons at room temperature, which is valuable for studying the multi-exciton physics in two-dimensional materials at room temperature and helpful for developing photonic devices based on monolayer TMDCs.

In Figure 1d, we show the in-plane electric field distribution calculated for a triangular $WS_2$ monolayer placed on the $Si_3N_4$/Ag heterostructure and excited by the TE wave. The TE wave propagates on the surface of the $Si_3N_4$ layer from left to right. It is noticed that a strong localization of the electric field is achieved at the front edges of the $WS_2$ monolayer, which is firstly excited by the TE wave. The enhancement factor is larger than that at the rear edge by a factor of ∼3.1. In order to see the influence of the $Si_3N_4$/Ag heterostructure on the emission properties of the excitons of the $WS_2$ monolayer, we calculated the emission intensities of a horizontally oriented dipole source placed on the $WS_2/Si_3N_4$/Ag heterostructure at different wavelengths. The result is shown in Figure 1e. The emission intensities of

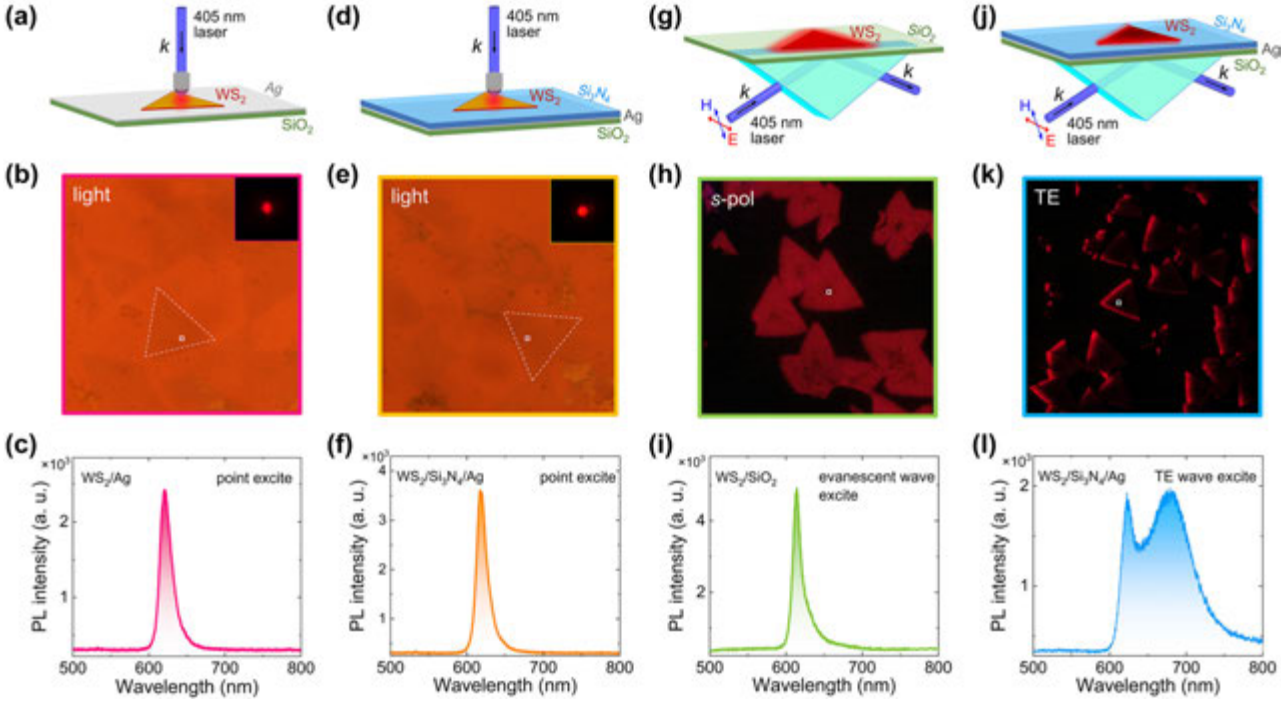


**Figure 2:** PL spectra of $WS_2$ monolayer on different substrate. (a) Schematic showing the excitation of a $WS_2$ monolayer placed on a Ag/$SiO_2$ substrate by using a focused laser light. (b) Optical image of the $WS_2$ monolayer (marked by a dashed triangle) placed on the Ag/$SiO_2$ substrate. The CCD image of the PL from the $WS_2$ monolayer is shown in the inset. (c) PL spectrum of the $WS_2$ monolayer placed on the Ag/$SiO_2$ substrate. (d) Schematic showing the excitation of a $WS_2$ monolayer placed on a $Si_3N_4$/Ag heterostructure by using a focused laser light. (e) Optical image of the $WS_2$ monolayer (marked by a dashed triangle) placed on the $Si_3N_4$/Ag heterostructure. The CCD image of the PL from the $WS_2$ monolayer is shown in the inset. (f) PL spectrum of the $WS_2$ monolayer placed on the $Si_3N_4$/Ag heterostructure. (g) Schematic showing the excitation of a $WS_2$ monolayer placed on a $SiO_2$ substrate by using the evanescent wave. (h) CCD image of triangular $WS_2$ monolayers placed on the $SiO_2$ substrate and excited by the evanescent wave. (i) PL spectrum of the $WS_2$ monolayer placed on the $SiO_2$ substrate and excited by the evanescent wave. (j) Schematic showing the excitation of a $WS_2$ monolayer placed on a $Si_3N_4$/Ag heterostructure by laser light coupled into the heterostructure as a TE wave. (k) CCD image of triangular $WS_2$ monolayers placed on the $Si_3N_4$/Ag heterostructure and excited by the TE wave. (l) PL spectrum of the $WS_2$ monolayer placed on the $Si_3N_4$/Ag heterostructure and excited by the TE wave.

the same dipole source placed on a $WS_2/SiO_2$ substrate is also provided for comparison. It is found that the emission intensity of the dipole source at ∼680 nm is enhanced by a factor of ∼5.0 as compared with that at ∼615 nm for the $WS_2$ monolayer placed on the $Si_3N_4$/Ag heterostructure. This behavior is not observed for the $WS_2$ monolayer placed on the $SiO_2$ substrate, implying that the exciton dynamics of the $WS_2$ monolayer can be modified by using the $Si_3N_4$/Ag heterostructure. As a result, the radiative recombination rate of the defect-bound excitons is greatly enhanced as compared with that of neutral excitons.

In order to understand the physical mechanisms responsible for the appearance of the defect-bound excitons in the PL spectrum of the $WS_2$ monolayer placed on $Si_3N_4$/Ag heterostructure and excited by the TE wave, we compare the PL spectra of $WS_2$ monolayers placed on different substrates and excited by different methods, as shown in Figure 2 (see Figure S3 in the Supporting Information). In Figure 2a–c, we show the PL measurement performed for a $WS_2$ monolayer placed on an $Ag/SiO_2$ substrate. The conventional point excitation and collection is employed in this case. Only a single peak (∼615 nm) originating from neutral excitons is observed [6, 9]. Similar result is found for the $WS_2$ monolayer placed on a $Si_3N_4$/Ag heterostructure if the same excitation method is employed, as shown in Figure 2d–f (see Figure S4 in the Supporting Information). Although the exciton dynamics is expected to be modified by the Ag film and the $Si_3N_4$/Ag heterostructure, the emission from defect-bound excitons is still invisible in the PL spectrum. This behavior indicates that the excitation of the entire the $WS_2$ monolayer instead of only a single point is crucial for revealing the emission from defect-bound excitons. For this reason, we also examined the PL spectrum of a $WS_2$ monolayer placed on a $SiO_2$ substrate and excited by using the evanescence wave, as shown in Figure 2g–i Unfortunately, the emission from defect-bound excitons is still very weak as compared with that of neutral excitons. It means that the modification in exciton dynamics is also necessary except the excitation of the entire $WS_2$ monolayer. These requirements are fulfilled for the $WS_2$ monolayer placed on $Si_3N_4$/Ag heterostructure, as shown in Figure 2j–l (see Figure S5 in the Supporting Information). In Figure 2l, one can clearly identify the emission from defect-bound excitons (∼680 nm) with intensity comparable to that from neutral excitons (∼615 nm) [6, 7, 9].

In order to confirm that the broad PL peak at ∼680 nm originates from the emission of defect-bound exciton, we perform PL measurements for a $WS_2$ monolayer at low temperatures, which is a conventional way to identify defect-bound excitons in monolayer TMDCs [6, 9]. In Figure 3a, we show the evolution of the PL spectrum of a $WS_2$ monolayer with decreasing temperature. It is noticed that the PL intensity is increased while the PL bandwidth is broadened with decreasing temperature. In Figure 3b, we show the PL spectrum obtained at $T = 50$ K together with the fitting with Lorentz lineshapes. One can see clearly the contributions from neural, charge, and bound excitons, which are denoted as $X_A$, $X_T$ and $X_D$, respectively. Although a blueshift of the PL peak is observed for all excitons at low temperatures, the similarity between the PL spectrum observed for the $WS_2$ monolayer placed on the $Si_3N_4$/Ag heterostructure and excited by the TE wave and that obtained at a low temperature confirms the revealing of $X_D$ at room temperature.

Now we investigate in detail the emission from defect-bound excitons ($X_D$) in the $WS_2$ monolayer placed on the $Si_3N_4$/Ag heterostructure and excited by the TE wave. Since the PL intensity on the $WS_2$ monolayer is not uniform, we first examine the PL spectra at different locations of the $WS_2$ monolayer, as shown in Figure 4a. The PL spectra obtained at different positions along the two dashed lines are shown in Figure 4b and c. It is found that the overall PL intensity decreases from the vertex (point 1) to the base

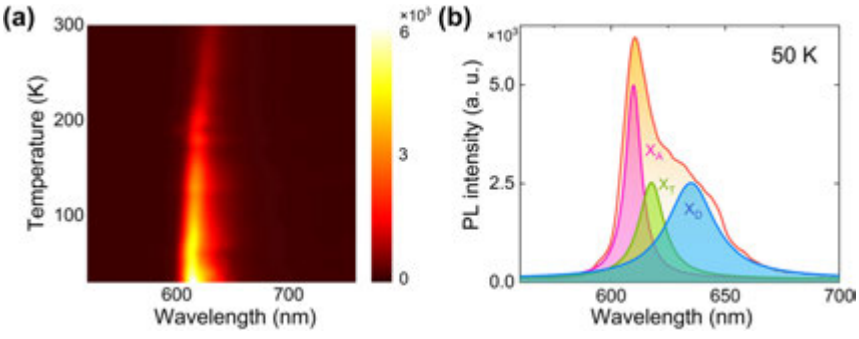


**Figure 3:** Low-temperature PL spectra of $WS_2$ monolayer. (a) Temperature-dependent PL spectra of a $WS_2$ monolayer placed on the $Si_3N_4$/Ag heterostructure and excited by a focused laser beam. (b) PL spectrum of the $WS_2$ monolayer placed on the $Si_3N_4$/Ag heterostructure obtained at $T = 50$ K. The fitting of the PL spectrum by using Lorentz lineshapes is also provided.

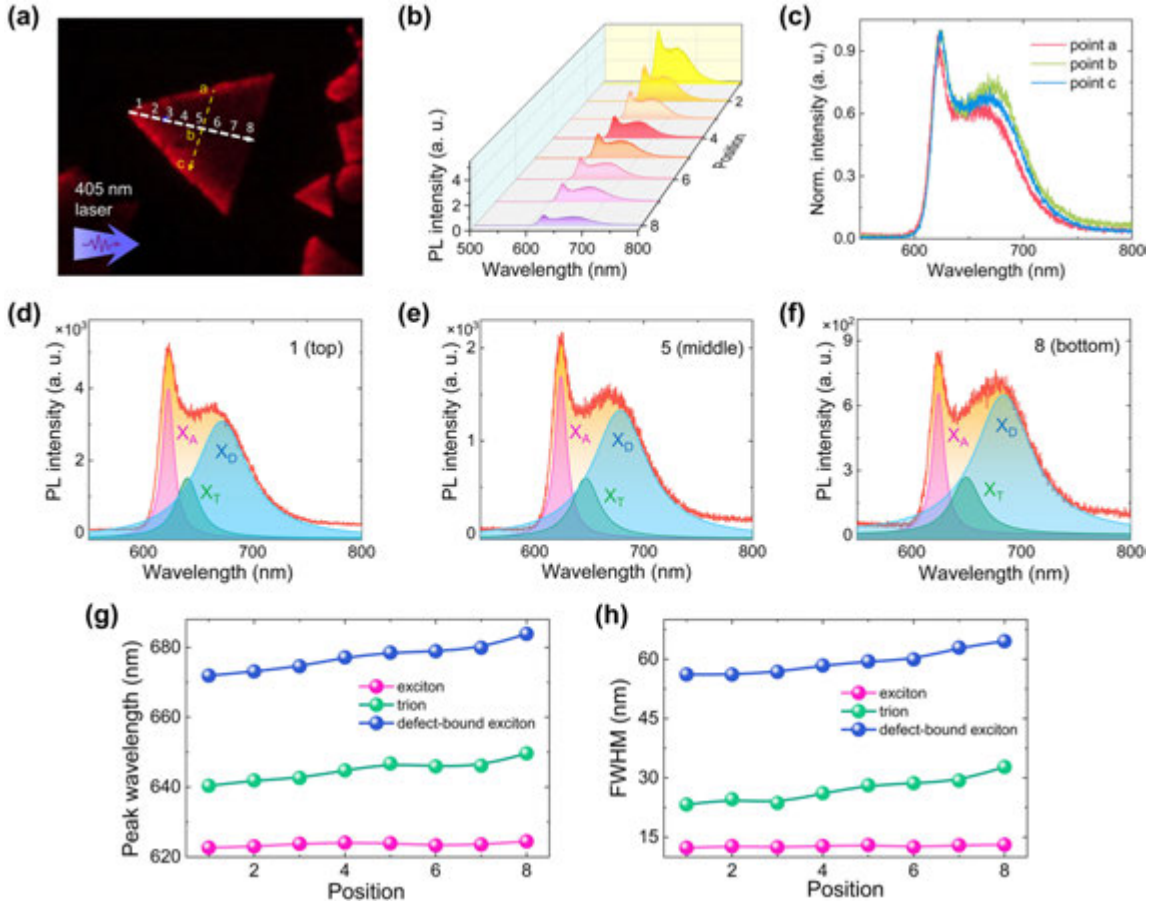


**Figure 4:** Efficiently exciting defect-bound excitons at different locations of the $WS_2$ monolayer by TE wave. (a) CCD image of a triangular $WS_2$ monolayer excited by 405-nm laser light coupled into the $Si_3N_4$/Ag heterostructure as a TE wave. The PL spectra are measured at different positions on the dashed line from the vertex (point 1) to the base (point 8) of the triangle and the dashed line parallel to the base of the triangle (point a-c). (b) PL spectra obtained at different positions (point 1–8) along the dashed line from the vertex to the base of the triangle. (c) The PL spectra obtained at different positions (point a–c) the dashed line parallel to the base of the triangle. (d–f) PL spectra measured at three different positions (point 1, 5, and 8) together with the fittings with multiple Lorentz lineshapes. (g) Position-dependent peak wavelength extracted for the three excitons ($X_A$, $X_T$, and $X_D$) from the fitting of the PL spectrum. (h) Position-dependent bandwidth extracted for the three excitons ($X_A$, $X_T$, and $X_D$) from the fitting of the PL spectrum.

(point 8) of the triangular $WS_2$ monolayer along the dashed line. However, it is noticed that the relative intensity of defect-bound excitons ($X_D$) with respect to that of neutral excitons ($X_A$) is increased. At point 8, the emission from $X_D$ becomes comparable to that from $X_A$. In comparison, no obvious change in the PL spectrum is observed along the other dashed line (from point a to point b), as shown in Figure 4c, implying that the emission from $X_D$ is sensitive to the propagation direction of the TE wave. In Figure 4d–f, we show the PL spectra obtained at three positions (point 1, 5, and 8) together with the fittings with multiple Lorentz lineshapes, which correspond to the emissions from $X_A$, $X_T$, and $X_D$, respectively. It can be seen that the contribution of $X_D$ becomes more significant at the dark region (point 8). In order to gain a deep insight into the change in the PL spectrum, we extracted the peak wavelengths and bandwidths of the three excitons observed at different positions, as shown in Figure 4g and h. It is found that both the wavelength and bandwidth of $X_A$ remain unchanged at different positions. In comparison, a redshift of the peak wavelength and a broadening of the bandwidth are observed for $X_T$ and $X_D$. The redshift and broadening appear to be more significant for $X_D$, implying the emissions from $X_D$ at different locations can be effectively collected at the base of the triangular $WS_2$ monolayer, which is the latest region excited by the propagating TE wave. Actually, the emission from neutral excitons couples strongly to the TE waveguide mode because of their in-plane transition dipole moments. However, the strong self-absorption effect makes it decay fast during propagation. In comparison, the weak

self-absorption for defect-bound excitons leads to a longer propagation distance, enhancing the emission from defect-bound excitons at the collection point. Thus, the nonlocal feature of defect-bound excitons makes it possible to reveal their emission in the PL spectrum of a $WS_2$ monolayer at room temperature.

So far, we have demonstrated that the emission from $X_D$ can be revealed in the PL spectrum of a $WS_2$ monolayer placed on a $Si_3N_4$/Ag heterostructure at room temperature by coupling the excitation laser light into the heterostructure as a TE wave. In practical applications, it is desirable that the relative intensity of $X_D$ can be manipulated by simply changing the excitation condition. In Figure 5a, we show the PL spectra obtained at position 8 by using different laser powers (see Figure S6 in the Supporting Information). It is remarkable that relative intensities of $X_A$, $X_T$, and $X_D$ can be modified by simply varying the laser power ($P$). Similarly, we can extract the integrated intensities ($I$) of $X_A$, $X_T$, and $X_D$ at different laser powers by fitting the PL spectrum with multiple Lorentz lineshapes. The dependence of the integrated intensity on the laser power derived for $X_A$, $X_T$, and $X_D$ are shown in Figure 5b–d, respectively. In all cases, the intensity increases rapidly at low laser powers ($P < 180$ mW) and slowly at high laser powers. Such a sublinear dependence on the laser power can be fitted by power law $I \propto P^k$ [41, 49, 50]. The parameter k extracted for $X_A$, $X_T$, and $X_D$ are ~0.19, ~0.11, and ~0.31, respectively. It is noticed that the slopes observed in the dependence of the emission intensity on the excitation power for all excitons are smaller than those observed in the conventional point excitation. Moreover, the slope observed for defect-bound excitons is even larger than that observed for neutral excitons. The rapid attenuation of neutral excitons induced by the strong self-absorption effect as compared with defect-bound excitons is responsible for this abnormal behavior. The complex fitting results indicate the nonuniform excitation of the $WS_2$ monolayer by the TE wave, implying the existence of multi-exciton channels in the emission (see Figure S7 in the Supporting Information). In Figure 5a, it is noticed that the peak wavelength of $X_D$ is blue-shifted with increasing the laser power. In contrast, the peak wavelength of $X_A$ peak remains almost unchanged. The blueshift is mainly caused by the band filling effect of defect states with increasing the excitation intensity [41, 51]. In Figure 5e and f, we present the dependences of the peak wavelength and bandwidth on the laser power extracted for the three

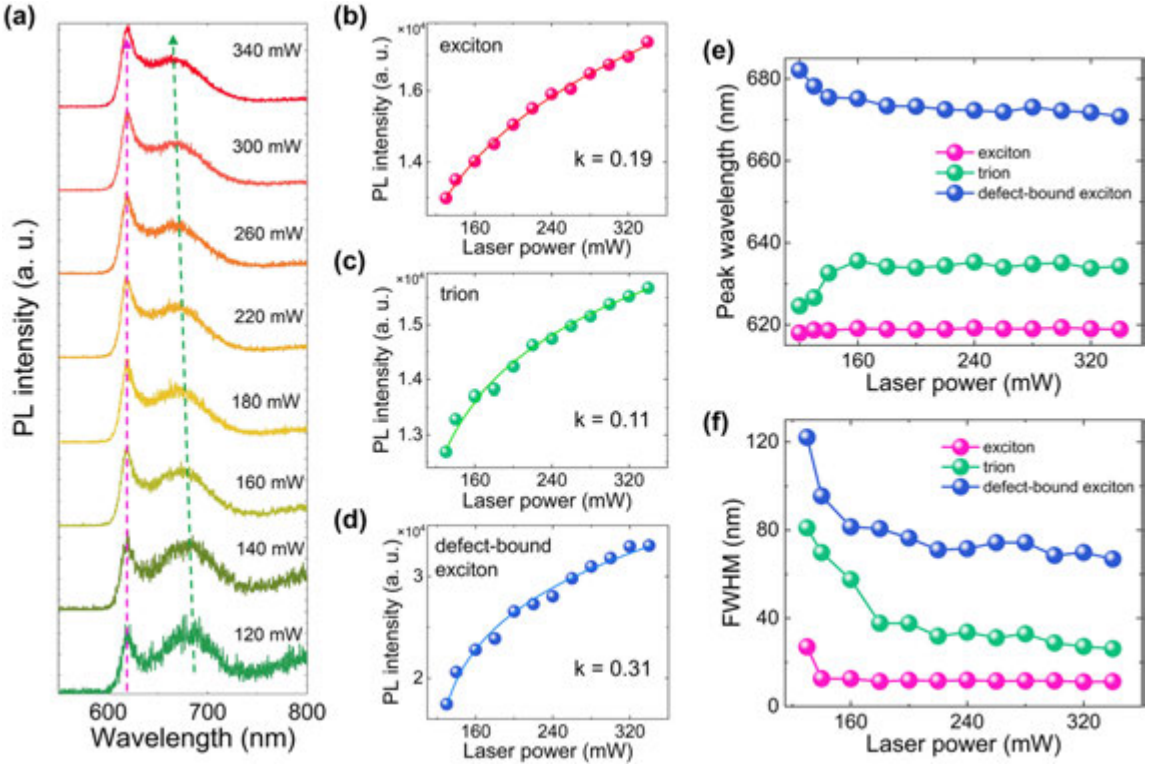


**Figure 5:** Manipulate the relative intensity of $X_D$ by change the excitation condition. (a) PL spectra of a $WS_2$ monolayer placed on the $Si_3N_4$/Ag heterostructure and excited by the TE wave with different laser powers. (b–d) Power-dependent integrated intensity extracted for $X_A$, $X_T$, and $X_D$ from the fitting of the PL spectra obtained at different laser powers. (e) Dependence of the peak wavelength on the laser power extracted for $X_A$, $X_T$, and $X_D$ from the fitting of the PL spectra obtained at different laser powers. (f) Dependence of the bandwidth on the laser power extracted for $X_A$, $X_T$, and $X_D$ from the fitting of the PL spectra obtained at different laser powers.

types of excitons. While a blueshift is observed for the peak wavelength of $X_D$, the peak wavelength of $X_T$ exhibits a redshift with increasing laser power. The peak wavelength of $X_A$ remains nearly unchanged. In all cases, one can see a narrowing of the bandwidth with increasing laser power, particularly in the emissions of $X_T$ and $X_D$. Peak has the opposite change in the center wavelength with increasing the power. Both the change in the peak wavelength and bandwidth induced by the laser power indicate that the binding energy of electrons and holes can be renormalized by the excitation laser light, which is beneficial to the formation of defects by trapping oxygen. As a result, the emission from defect-bound excitons can be visualized even at room temperature. This process is similar to the introduction of defects in $WS_2$ monolayer by using high-energy electron beam, revealing the emission of $X_D$ at room temperature [52] (see Figure S8 in the Supporting Information). In this case, however, the structure of the $WS_2$ monolayer is modified, limiting it practical applications.

# 3 Conclusions

In conclusion, we investigated the PL spectrum of a $WS_2$ monolayer placed on a $Si_3N_4$/Ag heterostructure and excited by coupling 405-nm laser light into the heterostructure as a TE wave. By utilising the TE wave to excite the entire $WS_2$ monolayer, modifying the exciton dynamics through the heterostructure, and enabling emission propagation along the waveguide structure, we successfully revealed the emission from defect-bound excitons at room temperature. We observed that the intensity of the defect-bound excitons strongly depends on the position along the propagating direction of the excitation TE wave and can be comparable to that of other excitons. Furthermore, we demonstrated that the relative intensity, peak wavelength, and bandwidth of the defect-bound excitons can be manipulated by simply adjusting the excitation laser power. Our findings highlight the advantages of dielectric-metal heterostructures in exciting defect-bound excitons, which are valuable for studying the multi-exciton physics in two-dimensional materials at room temperature and hold significance for the development of photonic devices based on monolayer TMDCs.

# 4 Methods

## 4.1 Sample preparation and characterization

In this work, the $WS_2/Si_3N_4$/Ag heterostructure was fabricated by using the method reported previously [48]. First, a 50-nm-thick Ag film was deposited on a silica ($SiO_2$) substrate by using electron beam evaposition. Then, a 100-nm-thick $Si_3N_4$ layer was deposited on the Ag film via high-frequency plasma-enhanced chemical vapor deposition (HF-PECVD). Finally, triangular $WS_2$ monolayers grown by the CVD method were transferred onto the surface of the $Si_3N_4$/Ag heterostructure. The morphologies of $WS_2$ monolayers were examined by SEM observation (Gemini 500, Zeiss). The density of defects was controlled by adjusting the irradiation time of the high-energy electron beam.

## 4.2 Optical characterization

The optical images and the PL spectra of $WS_2$ monolayer placed on different substrates were measured by using an inverted microscope (Axio Observer A1, Zeiss) equipped with a spectrometer (SR-500i-B1, Andor) and a color charge coupled device (CCD) (DS-Ri2, Nikon). Two methods were employed to excite the $WS_2$ monolayers placed on the $Si_3N_4$/Ag heterostructure. In the conventional excitation method, a 405-nm laser beam was introduced into the microscope and focused on $WS_2$ monolayers by using a 100× objective. In the excitation by using the TE wave, the 405-nm laser beam was coupled into the $Si_3N_4$/Ag heterostructure as a TE wave by using a prism, as schematically shown in Figure 1a. In both cases, the PL from the $WS_2$ monolayer was collected by using a 100× objective and directed to the spectrometer for analysis. The temperature-dependent PL spectra were measured using an Ultra-low vibration closed cycle cryostat (DE204PF-DMX-20-OM, ARS).

## 4.3 Numerical simulation

The numerical simulations were performed by using the finite-difference time-domain (FDTD) method (FDTD solution, https://www.lumerical.com). In the numerical simulation, the refractive index of $Si_3N_4$ was based on the measured data. The dielectric constants of Ag and $WS_2$ monolayer were taken from the previous literature [53, 54]. The thickness of the $WS_2$ monolayer was set to be 1.0 nm. The refractive index of the surrounding media was chosen to be 1.0. The dipole source was placed inside the $WS_2$ monolayer to calculate the radiation intensity of the $WS_2/Si_3N_4$/Ag heterostructure. The *p*- and *s*-polarized plane waves were used to calculate the electric and magnetic field distributions of TM and TE waves supported by Ag film and $Si_3N_4$/Ag heterostructures, respectively. The smallest mesh size as small as 0.5 nm was used to obtain converged simulation results, and perfectly matched layer boundary condition was employed to terminate the finite simulation.

**Research funding:** S. Lan acknowledges the National Natural Science Foundation of China (Grant No. 12174123). S. Li acknowledges the Natural Science Foundation of Guangdong Province (Grant No. 2022A1515010747) and the Start-Up Funding of Guangdong Polytechnic Normal University (2022SDKYA007). J. Xiang acknowledges the National Natural Science Foundation of China (Grant Nos. 62305035).
**Author contributions:** All authors have accepted responsibility for the entire content of this manuscript and approved its submission.
**Conflict of interest:** Authors state no conflicts of interest.
**Informed consent:** Informed consent was obtained from all individuals included in this study.

**Ethical approval:** The conducted research is not related to either human or animals use.

**Data availability:** Data sharing is not applicable to this article as no datasets were generated or analysed during the current study.

## References


[1] S. Wu, S. Buckley, J. R. Schaibley, et al., "Monolayer semiconductor nanocavity lasers with ultralow thresholds," *Nature*, vol. 520, no. 7545, pp. 69—72, 2015.

[2] Y. Ye, Z. J. Wong, X. Lu, et al., "Monolayer excitonic laser," *Nat. Photonics*, vol. 9, no. 11, pp. 733—737, 2015.

[3] Q. Guo, Z. Ou, J. Tang, et al., "Efficient frequency mixing of guided surface waves by atomically thin nonlinear crystals," *Nano Lett.*, vol. 20, no. 11, pp. 7956—7963, 2020.

[4] N. Kumar, S. Najmaei, Q. Cui, et al., "Second harmonic microscopy of monolayer MoS 2," *Phys. Rev. B*, vol. 87, no. 16, p. 161403, 2013.

[5] D.-H. Lien, S. Z. Uddin, M. Yeh, et al., "Electrical suppression of all nonradiative recombination pathways in monolayer semiconductors," *Science*, vol. 364, no. 6439, pp. 468—471, 2019.

[6] R. Kesarwani, K. B. Simbulan, T.-D. Huang, et al., "Control of trion-to-exciton conversion in monolayer WS2 by orbital angular momentum of light," *Sci. Adv.*, vol. 8, no. 13, p. eabm0100, 2022.

[7] Z. Luo, W. Zheng, N. Luo, et al., "Photoluminescence lightening: extraordinary oxygen modulated dynamics in WS2 monolayers," *Nano Lett.*, vol. 22, no. 5, pp. 2112—2119, 2022.

[8] R. Roldán, J. A. Silva-Guillén, M. P. López-Sancho, F. Guinea, E. Cappelluti, and P. Ordejón, "Electronic properties of single-layer and multilayer transition metal dichalcogenides MX2 (M= Mo, W and X= S, Se)," *Ann. Phys.*, vol. 526, nos. 9—10, pp. 347—357, 2014.

[9] K. Wu, H. Zhong, Q. Guo, et al., "Revealing the competition between defect-trapped exciton and band-edge exciton photoluminescence in monolayer hexagonal WS2," *Adv. Opt. Mater.*, vol. 10, no. 6, p. 2101971, 2022.

[10] Z. Ye, T. Cao, K. O'brien, et al., "Probing excitonic dark states in single-layer tungsten disulphide," *Nature*, vol. 513, no. 7517, pp. 214—218, 2014.

[11] K. He, N. Kumar, L. Zhao, et al., "Tightly bound excitons in monolayer WSe 2," *Phys. Rev. Lett.*, vol. 113, no. 2, p. 026803, 2014.

[12] L. Huang, G. Li, A. Gurarslan, et al., "Atomically thin MoS2 narrowband and broadband light superabsorbers," *ACS Nano*, vol. 10, no. 8, pp. 7493—7499, 2016.

[13] A. Splendiani, L. Sun, Y. Zhang, et al., "Emerging photoluminescence in monolayer MoS2," *Nano Lett.*, vol. 10, no. 4, pp. 1271—1275, 2010.

[14] D. Zheng, S. Zhang, Q. Deng, M. Kang, P. Nordlander, and H. Xu, "Manipulating coherent plasmon—exciton interaction in a single silver nanorod on monolayer WSe2," *Nano Lett.*, vol. 17, no. 6, pp. 3809—3814, 2017.

[15] J. Wen, H. Wang, W. Wang, et al., "Room-temperature strong light—matter interaction with active control in single plasmonic nanorod coupled with two-dimensional atomic crystals," *Nano Lett.*, vol. 17, no. 8, pp. 4689—4697, 2017.

[16] F. Deng, H. Liu, L. Xu, S. Lan, and A. E. Miroshnichenko, "Strong exciton—plasmon coupling in a WS2 monolayer on Au film hybrid structures mediated by liquid Ga nanoparticles," *Laser Photonics Rev.*, vol. 14, no. 4, p. 1900420, 2020.

[17] L. Huang, A. Krasnok, A. Alú, Y. Yu, D. Neshev, and A. E. Miroshnichenko, "Enhanced light—matter interaction in two-dimensional transition metal dichalcogenides," *Rep. Prog. Phys.*, vol. 85, no. 4, p. 046401, 2022.

[18] H. Huang, F. Deng, J. Xiang, S. Li, and S. Lan, "Plasmon-exciton coupling in dielectric-metal hybrid nanocavities with an embedded two-dimensional material," *Appl. Surf. Sci.*, vol. 542, p. 148660, 2021.

[19] F. Deng, H. Huang, J.-D. Chen, et al., "Greatly enhanced plasmon—exciton coupling in si/ws2/au nanocavities," *Nano Lett.*, vol. 22, no. 1, pp. 220—228, 2021.

[20] C. Cong, J. Shang, X. Wu, et al., "Synthesis and optical properties of large-area single-crystalline 2D semiconductor WS2 monolayer from chemical vapor deposition," *Adv. Opt. Mater.*, vol. 2, no. 2, pp. 131—136, 2014.

[21] J.-G. Song, J. Park, W. Lee, et al., "Layer-controlled, wafer-scale, and conformal synthesis of tungsten disulfide nanosheets using atomic layer deposition," *ACS Nano*, vol. 7, no. 12, pp. 11333—11340, 2013.

[22] Q. Liang, Q. Zhang, X. Zhao, M. Liu, and A. T. S. Wee, "Defect engineering of two-dimensional transition-metal dichalcogenides: applications, challenges, and opportunities," *ACS Nano*, vol. 15, no. 2, pp. 2165—2181, 2021.

[23] Z. Hu, Z. Wu, C. Han, J. He, Z. Ni, and W. Chen, "Two-dimensional transition metal dichalcogenides: interface and defect engineering," *Chem. Soc. Rev.*, vol. 47, no. 9, pp. 3100—3128, 2018.

[24] N. Peimyoo, J. Shang, C. Cong, et al., "Nonblinking, intense two-dimensional light emitter: monolayer WS2 triangles," *ACS Nano*, vol. 7, no. 12, pp. 10985—10994, 2013.

[25] H. R. Gutiérrez, N. Perea-López, A. L. Elías, et al., "Extraordinary room-temperature photoluminescence in triangular WS2 monolayers," *Nano Lett.*, vol. 13, no. 8, pp. 3447—3454, 2013.

[26] Z. Lin, A. McCreary, N. Briggs, et al., "2D materials advances: from large scale synthesis and controlled heterostructures to improved characterization techniques, defects and applications," *2D Mater.*, vol. 3, no. 4, p. 042001, 2016.

[27] S. Tongay, J. Suh, C. Ataca, et al., "Defects activated photoluminescence in two-dimensional semiconductors: interplay between bound, charged and free excitons," *Sci. Rep.*, vol. 3, no. 1, p. 2657, 2013.

[28] T. He, Z. Wang, R. Cao, et al., "Extrinsic photoconduction induced short-wavelength infrared photodetectors based on Ge-based chalcogenides," *Small*, vol. 17, no. 4, p. 2006765, 2021.

[29] J. S. Ross, S. Wu, H. Yu, et al., "Electrical control of neutral and charged excitons in a monolayer semiconductor," *Nat. Commun.*, vol. 4, no. 1, p. 1474, 2013.

[30] S. Radautsan and I. Tiginyanu, "Defect engineering in II—III2—VI4 and related compounds," *Jpn. J. Appl. Phys.*, vol. 32, no. S3, p. 5, 1993.

[31] M. Zhou, W. Wang, J. Lu, and Z. Ni, "How defects influence the photoluminescence of TMDCs," *Nano Res.*, vol. 14, pp. 29—39, 2021.

[32] J. Xiong, J. Di, J. Xia, W. Zhu, and H. Li, "Surface defect engineering in 2D nanomaterials for photocatalysis," *Adv. Funct. Mater.*, vol. 28, no. 39, p. 1801983, 2018.

[33] A. Soni, D. Kushavah, L.-S. Lu, W. H. Chang, and S. K. Pal, "Ultrafast exciton trapping and exciton—exciton annihilation in large-area CVD-grown monolayer WS2," *J. Phys. Chem. C*, vol. 125, no. 43, pp. 23880—23888, 2021.

[34] S. Ippolito, A. G. Kelly, R. Furlan de Oliveira, et al., "Covalently interconnected transition metal dichalcogenide networks via defect engineering for high-performance electronic devices," *Nat. Nanotechnol.*, vol. 16, no. 5, pp. 592—598, 2021.
[35] A. W. Robertson, C. S. Allen, Y. A. Wu, et al., "Spatial control of defect creation in graphene at the nanoscale," *Nat. Commun.*, vol. 3, no. 1, p. 1144, 2012.
[36] P. K. Chow, R. B. Jacobs-Gedrim, J. Gao, et al., "Defect-induced photoluminescence in monolayer semiconducting transition metal dichalcogenides," *ACS Nano*, vol. 9, no. 2, pp. 1520—1527, 2015.
[37] K. Wu, Z. Li, J. Tang, et al., "Controllable defects implantation in MoS 2 grown by chemical vapor deposition for photoluminescence enhancement," *Nano Res.*, vol. 11, pp. 4123—4132, 2018.
[38] K. Parto, S. I. Azzam, K. Banerjee, and G. Moody, "Defect and strain engineering of monolayer WSe2 enables site-controlled single-photon emission up to 150 K," *Nat. Commun.*, vol. 12, no. 1, p. 3585, 2021.
[39] Z. Wu, W. Zhao, J. Jiang, et al., "Defect activated photoluminescence in WSe2 monolayer," *J. Phys. Chem. C*, vol. 121, no. 22, pp. 12294—12299, 2017.
[40] J. Shim, A. Oh, D. H. Kang, et al., "High-performance 2D rhenium disulfide (ReS2) transistors and photodetectors by oxygen plasma treatment," *Adv. Mater.*, vol. 28, no. 32, pp. 6985—6992, 2016.
[41] Z. Wu and Z. Ni, "Spectroscopic investigation of defects in two-dimensional materials," *Nanophotonics*, vol. 6, no. 6, pp. 1219—1237, 2017.
[42] M. Wang, A. Krasnok, T. Zhang, et al., "Fano resonances: tunable fano resonance and plasmon—exciton coupling in single Au nanotriangles on monolayer WS2 at room temperature (adv. Mater. 22/2018)," *Adv. Mater.*, vol. 30, no. 22, p. 1870155, 2018.
[43] J. Fang, K. Yao, T. Zhang, et al., "Room-temperature observation of near-intrinsic exciton linewidth in monolayer WS2," *Adv. Mater.*, vol. 34, no. 15, p. 2108721, 2022.
[44] G. Hu, X. Hong, K. Wang, et al., "Coherent steering of nonlinear chiral valley photons with a synthetic Au—WS2 metasurface," *Nat. Photonics*, vol. 13, no. 7, pp. 467—472, 2019.
[45] L. Yuan, J. Jeong, K. W. Chi Kwock, et al., "Manipulation of exciton dynamics in single-layer WSe2 using a toroidal dielectric metasurface," *Nano Lett.*, vol. 21, no. 23, pp. 9930—9938, 2021.
[46] Q. Guo, B. Wu, R. Du, et al., "Boosting exciton transport in WSe2 by engineering its photonic substrate," *ACS Photonics*, vol. 9, no. 8, pp. 2817—2824, 2022.
[47] S. Li, L. Zhou, M. Panmai, J. Xiang, and S. Lan, "Magnetic plasmons induced in a dielectric-metal heterostructure by optical magnetism," *Nanophotonics*, vol. 10, no. 10, pp. 2639—2649, 2021.
[48] S. Li, L. Zhou, F. Deng, et al., "Transverse-electric-polarized polaritons propagating in a WS2/Si3N4/Ag heterostructure," *Laser Photonics Rev.*, vol. 16, no. 12, p. 2100457, 2022.
[49] Z. Wu, Z. Luo, Y. Shen, et al., "Defects as a factor limiting carrier mobility in WSe2: a spectroscopic investigation," *Nano Res.*, vol. 9, no. 12, pp. 3622—3631, 2016.
[50] T. Schmidt, K. Lischka, and W. Zulehner, "Excitation-power dependence of the near-band-edge photoluminescence of semiconductors," *Phys. Rev. B*, vol. 45, no. 16, p. 8989, 1992.
[51] H. Qiu, T. Xu, Z. Wang, et al., "Hopping transport through defect-induced localized states in molybdenum disulphide," *Nat. Commun.*, vol. 4, no. 1, p. 2642, 2013.
[52] G. Delie, P. M. Litwin, S. J. McDonnell, D. Chiappe, M. Houssa, and V. V. Afanas'ev, "Energy Band Alignment of Few-Monolayer WS2 and WSe2 with SiO2 Using Internal Photoemission Spectroscopy," *ECS J. Solid State Sci. Technol.*, vol. 9, no. 9, p. 093009, 2020.
[53] P. B. Johnson and R.-W. Christy, "Optical constants of the noble metals," *Phys. Rev. B*, vol. 6, no. 12, p. 4370, 1972.
[54] Y. Li, A. Chernikov, X. Zhang, et al., "Measurement of the optical dielectric function of monolayer transition-metal dichalcogenides: MoS 2, Mo S e 2, WS 2, and WS e 2," *Phys. Rev. B*, vol. 90, no. 20, p. 205422, 2014.

**Supplementary Material:** This article contains supplementary material (https://doi.org/10.1515/nanoph-2023-0560).